11 Friction of the Smectite Clay Montmorillonite

A Review and Interpretation of Data

Diane E. Moore and David A. Lockner

Abstract

Previous frictional strength experiments on the smectite clay montmorillonite conducted under supposedly similar conditions have yielded apparent values of the coefficient of friction μ (the shear stress/effective normal stress) that can range from 0.06 to 0.78. We report some new laboratory data that illustrate that this wide variation is in part a function of the large difference in strength between thoroughly dried (μ ≥ 0.7) and water-saturated (μ ≤ 0.3) montmorillonite. Dry montmorillonite gouge is subject to standard frictional processes such as abrasion, wear, and fracture during shear. In contrast, shear of water-saturated montmorillonite gouge is concentrated in thin films of water that are adsorbed onto the (001) surfaces of the platy grains. The water-saturated shear strength of layer-structure minerals increases with the strength of the bonding of the polar water molecules to the (001) surfaces, and the relative weakness of water-saturated montmorillonite may be largely owing to its small layer charge. Published values of μ for montmorillonite that are considered to represent (deionized) water-saturated, equilibrated conditions increase regularly from 0.06 at effective normal stresses, $\sigma_n' < 1$ MPa to 0.30 at $\sigma_n' \approx 300$ MPa. The direct correlation of μ with effective stress is characteristic of sheet-silicate gouges, and it is attributed to decreasing thickness of the surface water films with increasing σ_n'. Increasing salinity of the pore fluid has the same effect on shear strength as increasing σ_n'. Most of the published strength data for montmorillonite fall outside the range of μ for water-saturated, equilibrated samples. Of these, the samples that are overly strong for a given set of experimental conditions may have been only partially saturated. The overly weak samples appear to be caused by inadequate drainage and consequent buildup of internal pore pressure. The velocity dependence of montmorillonite strength has not been extensively investigated. Water-saturated montmorillonite gouge

is velocity strengthening over the range of conditions tested to date, whereas partially saturated montmorillonite gouge may be velocity weakening at some velocities. These results highlight the hazards of interpreting fault-zone behavior based on experiments that do not approximate natural conditions. For example, the use of unsaturated clay rheology in modeling subducted sediment wedges in megathrust environments could lead to erroneous predictions.

Introduction

The smectite clay montmorillonite is an important low-temperature alteration product of mafic igneous volcanic rocks, particularly tuffs and volcanic ash [*Grim and Güven*, 1978]. Because of the close association of volcanic arcs with subduction zones, montmorillonite can be an important constituent of the accretionary wedges and downgoing sediments in subduction zones (see Table 1 of *Vrolijk* [1990, and references therein]). According to *Vrolijk* [1990], airborne volcanic ash incorporated into the hemipelagic deposits of the ocean basins alters to produce weak, smectite-rich horizons, along which the décollement may preferentially form as the oceanic crust is subducted. Localization of the décollement within smectite-rich units has been observed in the North Barbados [e.g., *Pudsey*, 1984; *Capet et al.*, 1990; *Tribble*, 1990] and Nankai [e.g., *Chamley et al.*, 1986] troughs. Along-strike variations in smectite-clay abundance in the décollement of the Cascadia subduction zone may control the vergence direction of thrust faults in the overlying accretionary wedge [*Underwood*, 2002].

Montmorillonite is also commonly found in other fault-zone settings [e.g., *Vrolijk and van der Pluijm*, 1999]. In particular, montmorillonite-bearing fault gouge has been identified in core from shallow drill holes into strike-slip faults such as the San Andreas fault system [*Wu et al.*, 1975; *Liechti and Zoback*, 1979] and the Nojima fault of Japan [*Ohtani et al.*, 2000]. Clays have been postulated to be present at considerable depths in some faults [*Wu et al.*, 1975; *Wu*, 1978], although montmorillonite may not be stable at temperatures above ≈150°C [e.g., *Abercrombie et al.*, 1994].

Since its identification as a low-strength mineral [*Kenney*, 1967; *Summers and Byerlee*, 1977a], montmorillonite has received considerable attention from the rock mechanics community as a possible cause of weak faults. Unfortunately, many of the published results are contradictory with respect to both frictional strength and the velocity dependence of friction. The purpose of this paper is to offer explanations for the apparent contradictions among the existing data, based on our recent investigations of the dry and water-saturated frictional strengths of sheet-structure minerals [*Moore and Lockner*, 2004] combined with the earlier work of *Wang et al.* [1980]. Assuming our interpretation is correct, this provides a framework for understanding the apparently inconsistent measurements of montmorillonite strength.

Summary of Existing Friction Data on Montmorillonite

Figure 11.1 summarizes the published friction data for montmorillonite (data sources are identified in figures 11.8 and 11.10). Where necessary, μ was calculated using the reported experimental conditions and stress measurements. The gap in the data between ~0.5 and 5 MPa separates the soil mechanics investigations conducted at very low-stress conditions from the higher-stress rock mechanics studies. The reported values of coefficient of friction μ at a given value of apparent effective normal stress σ_n' vary widely. For example, between 100 and 150 MPa σ_n', μ ranges from 0.06 to 0.78, more than an order of magnitude variation. This wide range is too large to be explained by differences in sample composition or systematic errors in test procedures.

Fewer measurements have been made of the velocity dependence of montmorillonite strength, but these too are contradictory. *Logan and Rauenzahn* [1987], *Morrow et al.* [1992], *Brown et al.* [2003], and D. A. Lockner and H. Tanaka (manuscript in preparation, 2006) measured solely velocity-strengthening behavior (shear strength increases with increasing velocity), whereas *Saffer et al.* [2001]
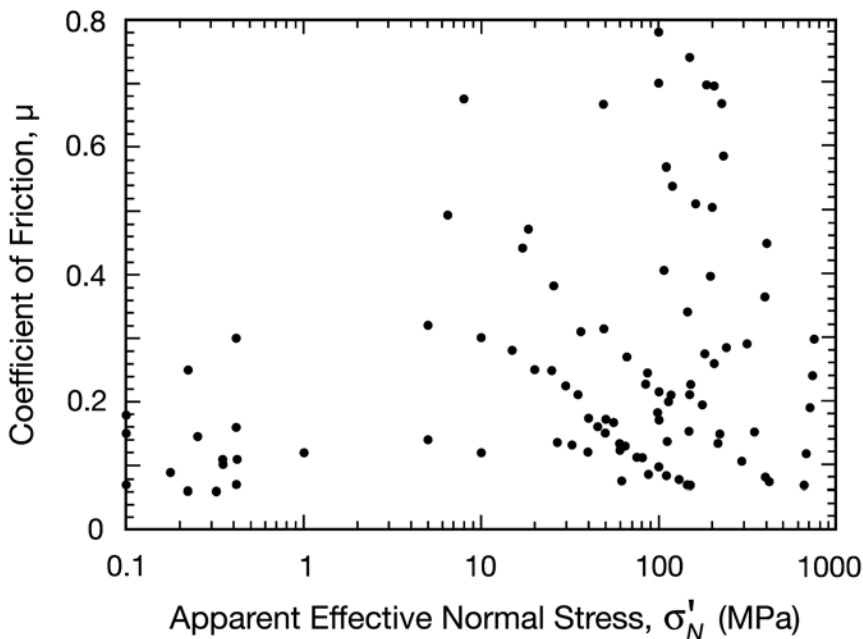

Figure 11.1 Compilation of room-temperature friction data for montmorillonite from soil- and rock-mechanics investigations (see fig. 11.8 and 11.10 for data sources). At a given apparent effective normal stress, reported coefficients of friction can vary by as much as 0.7.

reported that under certain conditions montmorillonite is velocity weakening (shear strength decreases with increasing velocity) and consequently capable of unstable slip.

If all these data are taken at face value, montmorillonite can be strong or weak, stable or unstable under reportedly similar conditions.

Experiments Conducted

We ran five triaxial friction experiments to illustrate some aspects of the frictional strength of montmorillonite. The starting material is a commercial montmorillonite clay, Volclay MPS-1, that has the composition: $Na_{0.3}(Fe^{+2},Mg)_{0.3}$ $(Al,Fe^{+3})_{1.7}Si_4O_{10}(OH)_2 \cdot nH_2O$. The grains are thin plates with vaguely hexagonal outlines and diameters generally ≤0.5 μm (fig. 11.2). The very fine grain size is typical of montmorillonite as is a large ratio of (001) surface area to grain thickness [e.g., *Güven*, 1988; *Tournassat et al.*, 2003]. The montmorillonite sample required no preparation for use as a gouge material.

For the experiments a 1.1-mm-thick layer of the montmorillonite gouge was placed along a 30° sawcut between 25.4-mm-diameter cylindrical driving blocks (fig. 11.3). Westerly granite was used for the lower forcing block in all five experiments and either Berea sandstone or Westerly granite for the upper block, which is located at the pore-fluid inlet. As figure 11.3 illustrates, the permeability of the upper forcing block is critical to good fluid communication
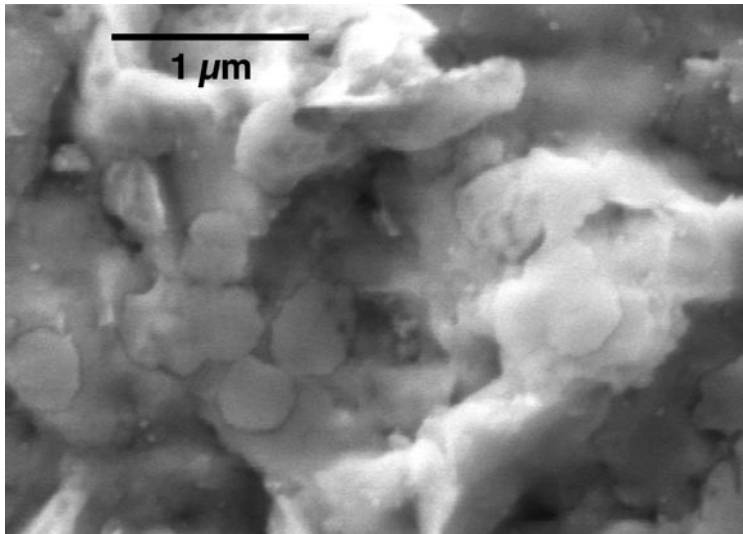

Figure 11.2 Secondary electron scanning electron microscope (SEM) image of the Na-montmorillonite MPS-1 starting material used in the experiments conducted for this study.
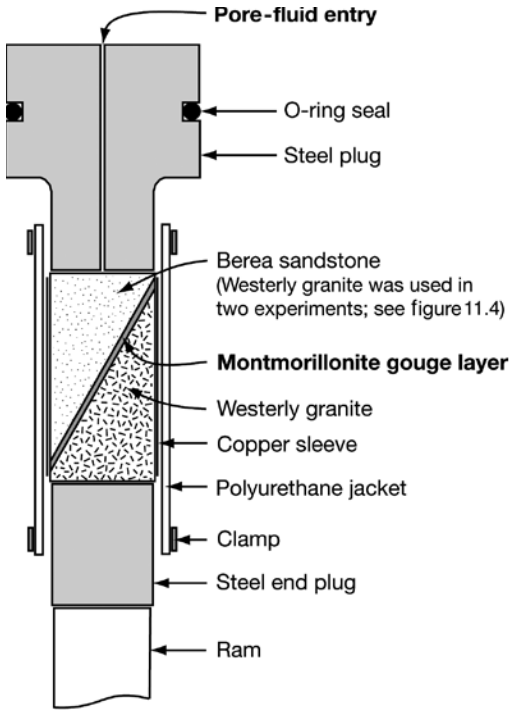
Figure 11.3   Sample assembly for tri-axial friction experiments.

between the gouge layer and the external pore-pressure system, and the two rock types were chosen to demonstrate this. On the one hand, Berea sandstone has a porosity of 18% and a relatively high permeability on the order of 10^{-13} m^2 [*Zoback and Byerlee*, 1975]. On the other hand, the permeability of Westerly granite is in the approximate range 10^{-20}–10^{-19} m^2 [*Morrow et al.*, 1986], 6–7 orders of magnitude lower than that of Berea sandstone.

The gouge layer was applied to one sawcut surface as a thick slurry, and the other block was placed on top of the gouge layer. The sample was inserted into a 0.05-mm-thick copper sleeve to keep the assembly intact; the copper sleeve ruptures during the initial 1–2 mm of shear and therefore does not contribute to the reported strengths. With one exception, the samples were vacuum-dried overnight (~22 hours) at 125°C, and upon removal from the oven, the dried samples were immediately jacketed and placed in the pressure vessel. The sample assembly and the pore-pressure lines were evacuated for ≥20 min. Confining pressure was then raised to the desired level; if the experiment was to be conducted under water-saturated conditions, the fluid pressure was applied after the confining pressure. Room-temperature velocity-stepping experiments were conducted at axial velocities of 0.05, 0.5, and 5.0 μm/s. Constant σ_n' was maintained in each experiment by means of computer-controlled adjustments to the confining pressure. The exception was a sample that was

Figure 11.4 Friction experiments on montmorillonite conducted for this study. (a) Con- ▶
trasting strengths of montmorillonite samples dried overnight at 125°C, one
run dry and the other run at 10-MPa pore pressure of deionized water.
Both samples used Berea sandstone as the forcing block adjoining the pore-
pressure inlet (fig. 11.3). Experiments were run at a sequence of axial velocities,
as indicated. (b) Velocity-stepping friction tests at 150 MPa σ_n', using sand-
stone/granite forcing blocks in one experiment and granite/granite forcing
blocks in the other two. (c) Enlargement of the strength tests between 3.5-
and 8.5-mm axial displacement, to better illustrate the changes in μ accom-
panying the velocity steps. Labels i–v identify the strength experiments from
figures 11.4a and 11.4b.

dried at 50°C for 3.5 hours, evacuated for 3 hours in the pressure vessel, and
allowed to sit overnight at the confining and pore-fluid pressure conditions of
the experiment prior to testing.

A prominent feature of montmorillonite friction is the very large difference
between dry and water-saturated strengths at the same effective normal stress
(fig. 11.4a). At 100 MPa σ_n', μ of thoroughly dry montmorillonite is roughly
4 times as large as that of water-saturated montmorillonite. Raising σ_n' from
100 to 150 MPa increases the water-saturated value of μ by ≈0.03 (fig. 11.4b).
The two experiments in figure 11.4b that used Westerly granite for the upper
forcing blocks were designed to illustrate how the low-permeability granite
increases the time needed to equilibrate pore-fluid pressure in the gouge layer.
The equilibration times were even longer than expected; when the samples
were disassembled immediately after the experiments, the sheared gouge lay-
ers showed no signs of dampness, even though the top of the upper granite
piece, adjacent to the pore-pressure inlet (fig. 11.3), was wet.

The changes in strength accompanying the velocity steps are briefly sum-
marized here. The two truly water-saturated samples (ii and v, the ones us-
ing sandstone/granite forcing-block pairs) are velocity strengthening over the
range tested, as better illustrated in the enlarged plots in figure 11.4c. The more
irregular strength behavior of the two samples with granite/granite blocks
(figs. 11.4b and 11.4c) made it difficult to determine accurately the change in
μ accompanying a velocity step. In all cases, however, the estimated range of
values indicated velocity-strengthening behavior, despite the series of small
stress drops that occurred during the 5-μm/s step of the sample dried at 125°C.
The strength of the dry sample, i (fig.11. 4c) is essentially independent of veloc-
ity within the uncertainty of the measurements.

Different shear-induced textures developed during the dry and water-
saturated experiments. Water-saturated gouge contains well-developed, shiny
and slickensided shear surfaces (fig. 11.5a), and (001) faces of the montmoril-
lonite grains in the shears are oriented parallel to the shear planes (fig. 11.5b).
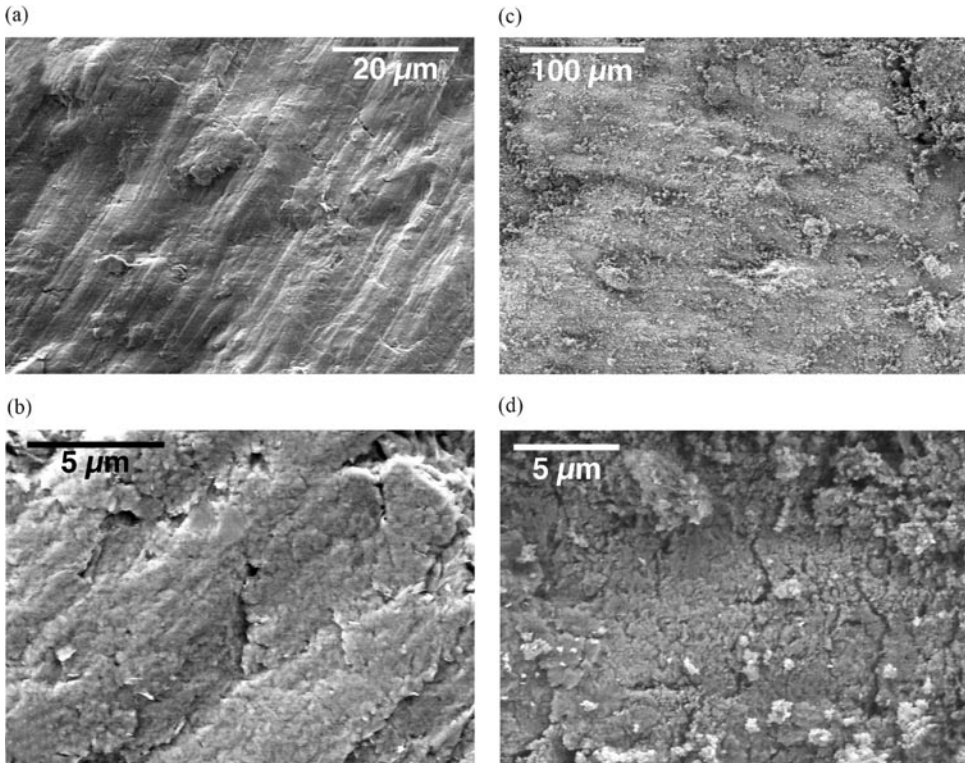Shear surfaces of the dry gouge sample tested at 100 MPa σ_n' (fig. 11.4a) are

(a)

(b)

(c)
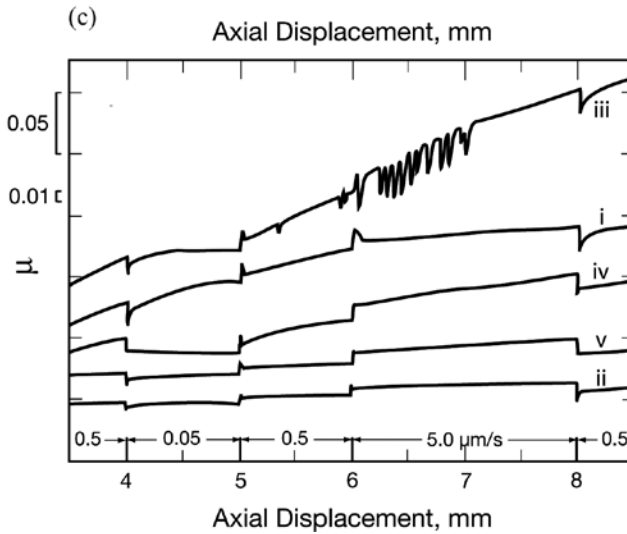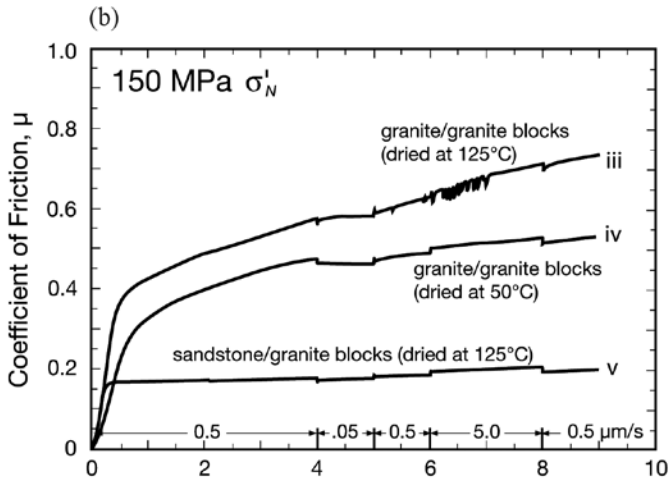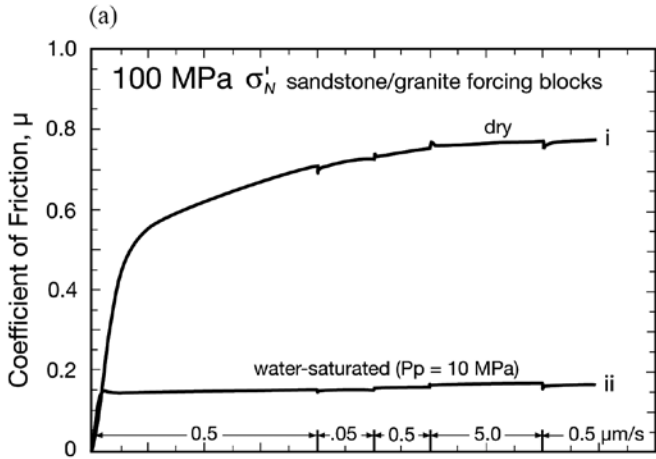
Figure 11.5 Secondary-electron SEM images of tested gouge samples. The water-saturated sample run at 150 MPa σ_n' shows good development of (a) shiny, slickensided shear surfaces characterized by (b) the strong preferred orientation of the platy montmorillonite grains parallel to the shear plane. The dry sample tested at 100 MPa σ_n' is characterized by (c) dull, grainy boundary-shear surfaces, although (d) grains in the shears have rotated into alignment with the shear surfaces.

considerably rougher and grainier in appearance (fig. 11.5c), and the preferred orientation of the platelets in the shears is only locally evident (fig. 11.5d).

Controls on Montmorillonite Frictional Strength

For layer-structured minerals such as the phyllosilicates, the bonding within a layer is strong whereas the bonds that hold the layers together (the (001) or interlayer bonds) are relatively weak. As a result, these minerals have a perfect cleavage parallel to (001) and usually a platy morphology (e.g., fig. 11.2). The relative weakness of the (001) bonds and the ensuing shape anisotropy are both important factors in controlling the frictional strengths of the layer-

structure minerals. In addition, dry and water-saturated shear of montmorillonite are characterized by the operation of different frictional processes that can cause their strengths to differ significantly.

Water-Saturated Friction

Water lubricates the shear of montmorillonite (fig. 11.4) and that of all other sheet-silicate minerals [*Horn and Deere*, 1962; *Moore and Lockner*, 2004]. Water attracted to the surfaces of the platelets forms thin, structured films with an integral number of layers when constrained between the basal planes of two adjoining sheet-silicate crystals [e.g., *Israelachvili, et al.*, 1988]. The films have a measurable shear strength that arises because the water molecules are bonded to the (001) surfaces of the crystals and also to the water molecules in other layers [*Israelachvili et al.*, 1988]. As illustrated in figures 11.5a and 11.5b, shear of water-saturated montmorillonite is localized to well-defined shear planes, and the platy grains in the shears have rotated so that their basal planes are parallel to the shear surfaces. Such deformation textures are characteristic of gouges composed of layer-structure minerals, and *Moore and Lockner* [2004] concluded that the shear of the phyllosilicate-rich gouges during their triaxial friction experiments was concentrated in the films of water adsorbed onto the (001) surfaces. Similar conclusions have been reached for the shear of clay sediments [e.g., *Rosenqvist*, 1984].

    The shear strength of the water films will be a function of the degree of attraction of the polar water molecules to the (001) surfaces; specifically, the strength is correlated with factors that contribute to the electrostatic component of the (001) interlayer bond [*Moore and Lockner*, 2004]. The smectite clays are 2:1 sheet silicates, in which a layer consists of an octahedral sheet sandwiched between two tetrahedral sheets. A net negative layer charge can arise in these minerals from substitutions in either the tetrahedral or octahedral sheet, and this charge is balanced by the addition of cations to the interlayer. On the basis of his calculations, *Giese* [1978] concluded that the layer charge is the major contributor to the (001) bond of the 2:1 sheet silicates. Because the tetrahedral sheet is always at the surface of a crystal in this mineral group, a water molecule should adhere more strongly to a 2:1 sheet silicate whose layer charge originates in the tetrahedral sheet [e.g., *Bleam*, 1990; *Skipper et al.*, 1993]. Consistent with this, the coefficient of friction correlates better with the tetrahedral-sheet charge (fig. 11.6) than with the total layer charge [*Moore and Lockner*, 2004]. Sheet-silicate minerals can be separated into two groups, trioctahedral and dioctahedral, based on the cations occupying the octahedral sheet. All of the octahedral cation sites of an ideal trioctahedral mineral are filled with divalent cations, whereas two thirds of the octahedral cation sites in a dioctahedral mineral are filled with trivalent cations and the other third are empty. A dioctahedral mineral always has somewhat stronger interlayer bonds than its trioctahedral equivalent [*Giese*, 1978], and the dioctahedral minerals in
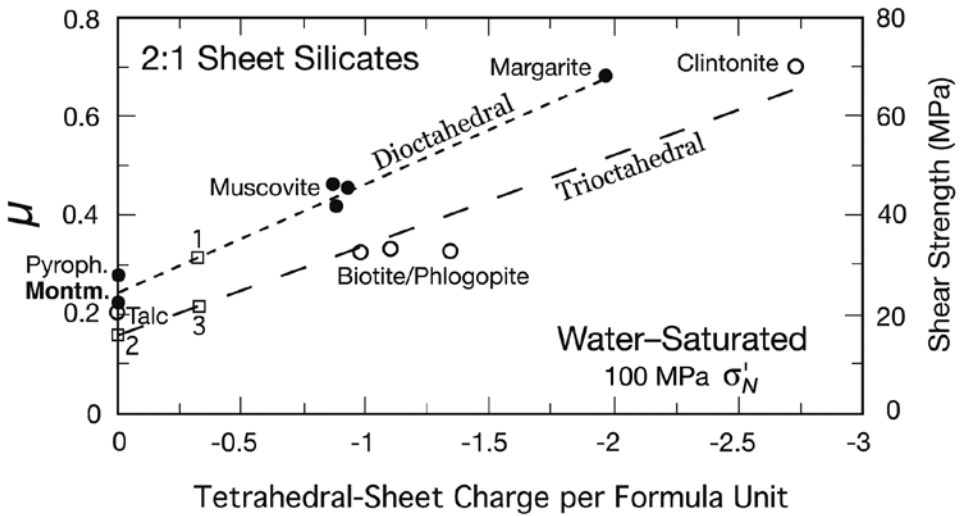
Figure 11.6   Correlation of water-saturated coefficient of friction of 2:1 sheet silicates at 100 MPa σ_n' with the charge on the tetrahedral sheets that form the surfaces of the (001) cleavage faces. Charge determinations were made using the measured composition of each mineral [*Moore and Lockner*, 2004]. For a given layer charge, μ is 0.10–0.15 larger for a dioctahedral mineral (solid circles) than for its trioctahedral (open circles) equivalent. The open squares labeled 1, 2, and 3 are the predicted values of μ for other smectite clays based on their ideal compositions: 1, beidellite and nontronite; 2, hectorite; 3, saponite.

figure 11.6 have consistently higher frictional strengths than their trioctahedral counterparts.

The coefficient of friction of water-saturated montmorillonite (fig. 11.6) is in accord with its 2:1 dioctahedral crystal structure, in which a small layer charge arises from substitutions in the octahedral rather than the tetrahedral sheet. Thus the strength of water-saturated montmorillonite gouge can be explained completely in terms of shear through the surface water films, as hypothesized for the other layer-structure minerals. The previous emphasis on the interlayer-water content of montmorillonite as the cause of its low strength [e.g., *Summers and Byerlee*, 1977a; *Bird*, 1984] may have arisen because the strengths of other very weak minerals such as the pyrophyllite and talc in figure 11.6 (both of them nonswelling minerals) had not yet been determined. Shear through surface water films of an expanded montmorillonite grain should always be easier than shear through its interlayer bonds, because the interlayer cations bind the layers together and generally limit the amount of expansion to <10 Å (1 nm). In contrast, the water films between separate platy grains can be considerably thicker [e.g., *Güven*, 1992; *Renard and Ortoleva*, 1997], particularly at $\sigma_n' < 100$ MPa (fig. 11.7a).

Dry Friction

The electrostatic components of the (001) bonds of many crystallographically well-characterized sheet-structure minerals were calculated by *Giese* [1978, 1980] and *Bish and Giese* [1981]. The coefficient of friction of thoroughly dried gouges of these minerals increases with increasing calculated (001) bond strength to values of ~70 kcal/mole [*Morrow et al.*, 2000; *Moore and Lockner*, 2004], at which point μ ≈ 0.8, satisfying "Byerlee's law" [*Byerlee*, 1978]. The coefficient of friction remains at ≈0.8 for minerals with bond strengths >70 kcal/mole. *Moore and Lockner* [2004] concluded that for those minerals with μ < 0.8, dry shearing occurs by cleaving through the (001) planes of the grains that have rotated into alignment with the shear planes. For the minerals with μ ≈ 0.8, shearing occurs by means of the frictional processes characteristic of "strong" minerals such as abrasion and wear, brittle fracture, and rolling [*Paterson*, 1978].

Because of the lack of a crystallographic structural refinement, the interlayer bond strength of montmorillonite has not been determined. However, on the basis of its overall crystal structure, dry montmorillonite was expected to be weaker than muscovite and biotite, for which μ (dry) at 100 MPa $σ_n'$ averages 0.59 and 0.54, respectively [*Moore and Lockner*, 2004]. Surprisingly, the dry montmorillonite sample in figure 11.4a has μ ≈ 0.8. The extremely fine grain size typical of montmorillonite clays and the very large area-to-thickness ratio may contribute to the unexpectedly high strength of dry montmorillonite. A montmorillonite grain that is only 1 unit cell thick [e.g., *Güven*, 1992; *Tournassat et al.*, 2003] cannot deform by cleaving through interlayer bonds. A minimum number of layers per crystal may be needed for the process to occur; thinner grains might preferentially flex or buckle rather than shear through (001). According to *Güven* [1992], montmorillonite lamellae only a few layers in thickness will often curl and fold. The grainy shear surfaces of the dry montmorillonite sample (figs. 11.5c and 11.5d) are similar to those of other phyllosilicates for which μ (dry) ≈ 0.8 [*Moore and Lockner*, 2004], suggesting that similar frictional processes were operative for all of them.

Interpretation of Published Strength Data on Montmorillonite

Water-Saturated, Equilibrated Strengths

To sort out the data in figure 11.1, we first identified those experiments that were conducted on water-saturated samples, with deionized water as the pore fluid, and that are considered to have maintained equilibrated fluid pressures during the tests. The data assigned to this group are shown in figure 11.7b. *Kenney* [1967], *Lupini et al.* [1981], and *Maio and Fenelli* [1994] conducted

Figure 11.7   (a) Thickness of water films between two platy crystal surfaces, calculated from
Debye-Hückel/osmotic theory, as a function of σ_n', from figure 11.4 of *Renard
and Ortoleva* [1997, p. 1968]. This curve is constructed for a mineral with a
surface charge energy of -0.01 C/m², at room temperature (25°C). (b) Com-
pilation of friction experiments that are considered to represent equilibrated,
water-saturated conditions using deionized water as pore fluid. The vertical bar
at the low-stress end is the range of μ from those experiments plotted in figure
11.8 that used deionized water. (c) Correlation of shear strengths calculated from
the data in figure 11.7b with the inverse of the calculated water-film thicknesses
from figure 11.7a at the effective normal stresses of the experiments.

direct-shear tests on montmorillonite at effective normal stresses in the range
0.1–0.5 MPa (fig. 11.8). They reported residual strengths, that is, the strengths
of the clay samples following the development of localized shears containing
aligned clay platelets [*Skempton*, 1964, 1985] similar to the one shown in figure
11.5a. Care was taken in all three studies to equilibrate the fluid pressure. The
reported values of μ from their experiments using pure water range between
0.06 and 0.11, as indicated by the vertical bar in figure 11.7b.

  All of the data at higher σ_n' are from triaxial friction experiments in which
Berea sandstone was the forcing block at the pore-pressure inlet. The high
permeability of Berea sandstone assures that the pore-pressure difference be-
tween the external control system and the sawcut surface of the gouge layer is
vanishingly small. The two sandstone/granite forcing-block experiments from
figure 11.4 are included in figure 11.7b, along with experiments from *Morrow
et al.* [1992, 2000] and D. A. Lockner and H. Tanaka (manuscript in preparation,
2006). Most of the data points from *Morrow et al.* [1992] included in figure 11.7b
are the averages of two to four tests conducted at different combinations of
fluid and confining pressures. Although some of their experiments were run
at high σ_n', thin sections of those samples show no evidence of damage to the
Berea sandstone forcing blocks. The data point from the *Morrow et al.* [2000]
paper is the final value of μ from an experiment that was run dry to 4-mm axial
displacement, then at 10-MPa pore-fluid pressure (100 MPa σ_n') to 9-mm axial
displacement. The reported values of μ from D. A. Lockner and H. Tanaka
(manuscript in preparation, 2006) are for a velocity of 1 μm/s, which is closest
to the velocities of the other high-σ_n' experiments in figure 11.7b.

  In figure 11.7b, μ increases relatively rapidly with increasing σ_n' at low
stress levels and then more slowly at higher stresses. The spread of values at
a given σ_n' reflects differences in experimental conditions such as the sliding
velocity and the amount of displacement. *Israelachvili et al.* [1988] determined
experimentally that the shear strength of a water film between two mica plates
increases as the number of water layers in the film decreases. This inverse re-
lation between water-film thickness and shear strength can be tested by com-
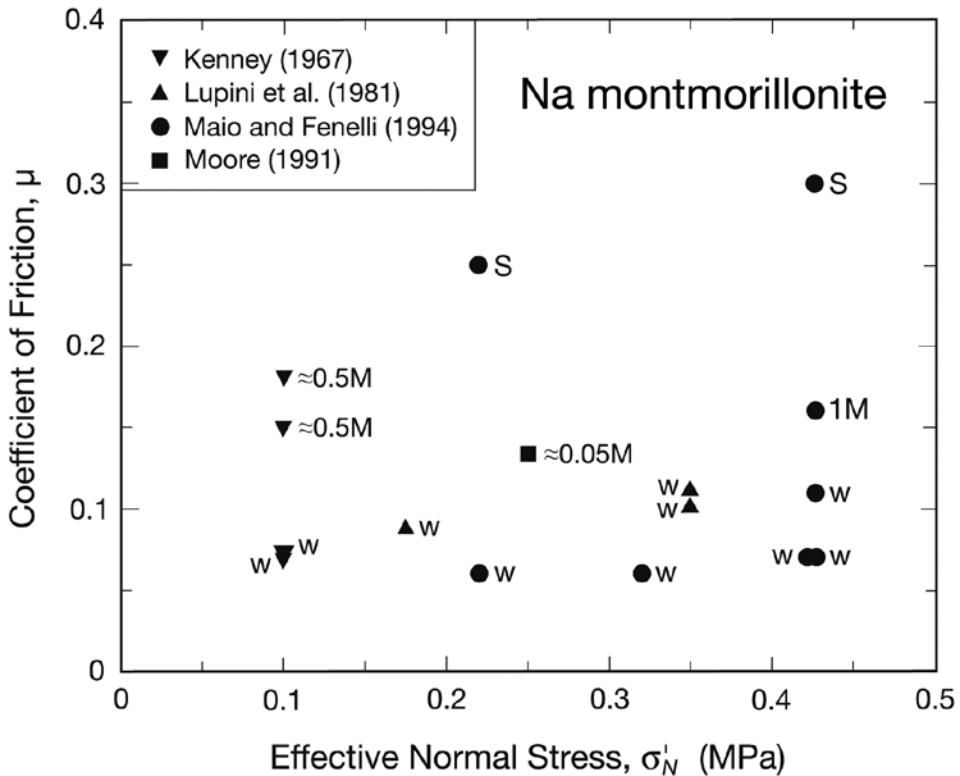
(a)

(b)

(c)
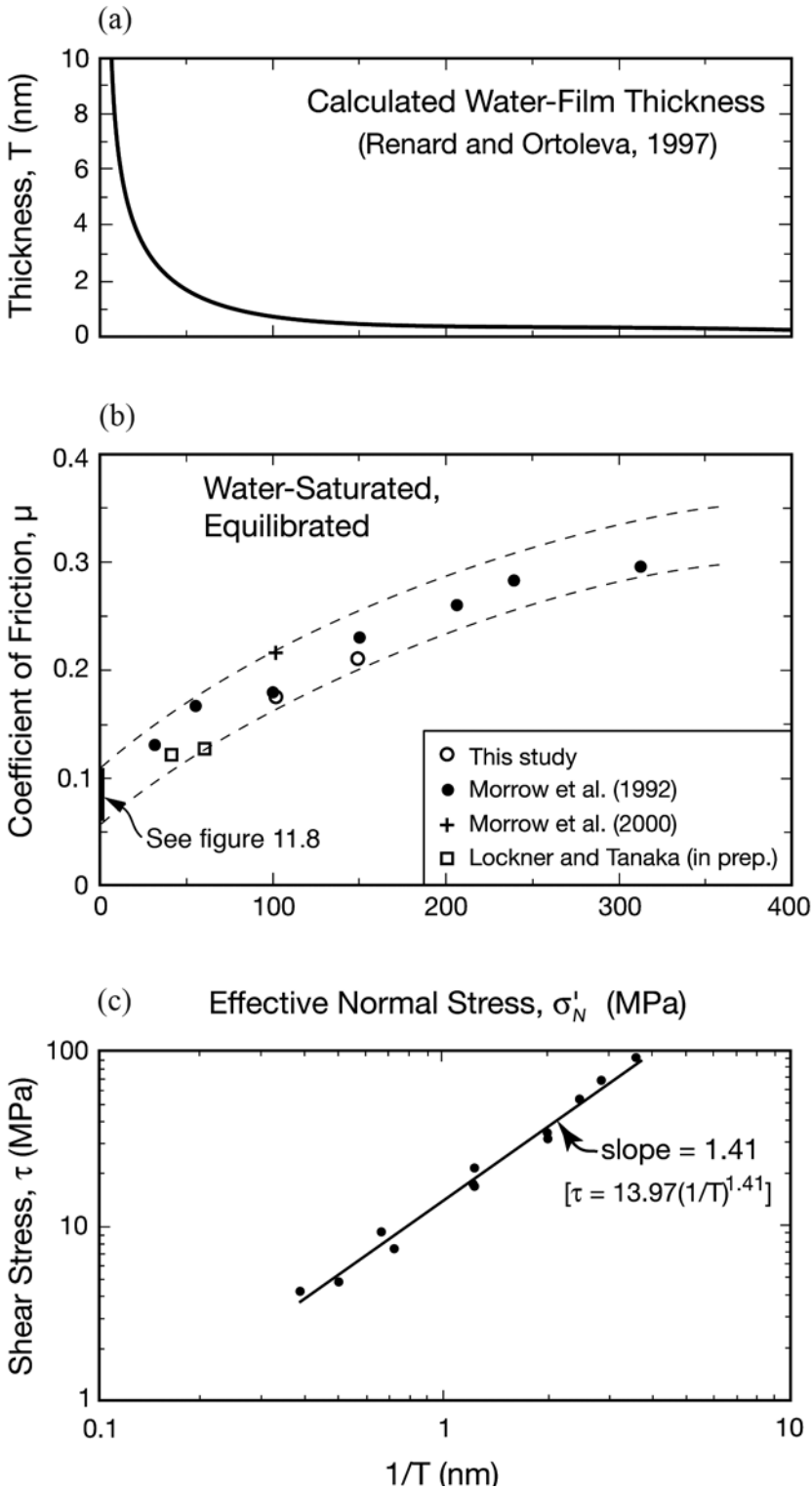
Figure 11.8   Coefficient of friction of Na-montmorillonite at $\sigma_n' < 0.5$ MPa, obtained from direct-shear and shear-box experiments. Labels: w, deionized or distilled water; ≈ 0.05 M, ≈ 0.5 M, 1 M = NaCl solutions of various concentrations; S, saturated NaCl solution.

paring clay shear strength ($\tau = \mu\sigma_n'$) in figure 11.7b with water-film thickness (figure 11.7a), as calculated by *Renard and Ortoleva* [1997]. The result, shown in figure 11.7c, is consistent with a model in which shear resistance increases at higher pressures where more weakly bound water layers are driven off. The effect of decreasing water-film thickness is thus to reduce the lubricating ability of the water film and, in consequence, to raise the frictional strength. This behavior contrasts to that of common rock-forming minerals such as quartz and feldspar (see fig. 11.7 of *Byerlee* [1978, p. 624]), for which μ decreases at effective pressures above ≈200 MPa, but it appears to be typical of water-saturated clay- and other phyllosilicate-rich gouges. For example, at room temperature the coefficient of friction of the serpentine mineral chrysotile increases from 0.17 to 0.32 with increasing σ_n' between 40 and 300 MPa [*Moore et al.*, 2004], a range that is nearly identical to that of montmorillonite (fig. 11.9). The differences between dry and water-saturated frictional strengths of the other two important serpentine minerals, lizardite and antigorite, are smaller than found
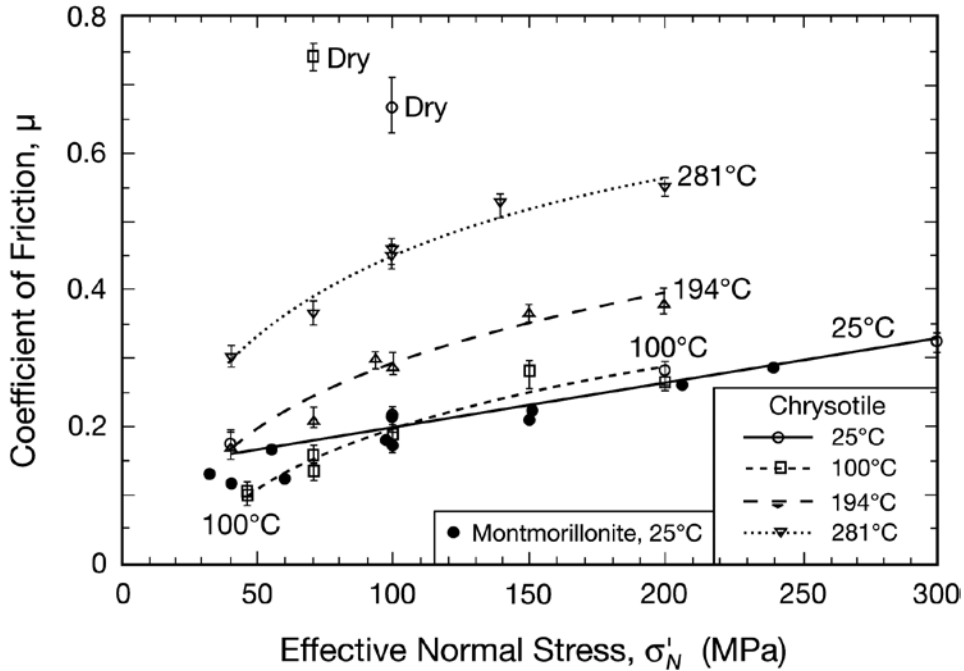
Figure 11.9   Variation of μ of the serpentine mineral chrysotile with temperature and σ_n', from *Moore et al.* [2004]. All but the two experiments labelled "Dry" were run under fluid-saturated conditions. The water-saturated, equilibrated montmorillonite friction data at $\sigma_n' > 30$ MPa from figure 11.7b are plotted for comparison. Room-temperature chrysotile and montmorillonite strengths are nearly identical over much of the range of effective normal stresses tested.

for chrysotile, and these two minerals are characterized by somewhat smaller rates of increase of μ with increasing σ_n' [*Moore et al.*, 1997]. The combined data of *Horn and Deere* [1962], *Kenney* [1967], and *Moore and Lockner* [2004] suggest that μ also increases with σ_n' for water-saturated muscovite, biotite, chlorite, kaolinite, and talc.

Other Experiments

The data set from figure 11.1 is replotted in figure 11.10a with the field of water-saturated, equilibrated montmorillonite strengths from figure 11.7b, labeled "Saturated," superimposed on it. Another field labeled "Dry Strength" at μ ≥ 0.7 is defined by the dry experiment from figure 4a and the dry value of μ for montmorillonite reported by *Morrow et al.* [2000]. The granite/granite sample from figure 11.4b that was dried at 125°C plots with the dry samples despite the introduction of water to the top of the upper granite cylinder (fig. 11.3). In compiling the available friction data on rocks and rock-forming

Figure 11.10   Interpretations of the data presented in figure 11.1, plotting (a) apparent coef- ▶
ficient of friction against apparent effective normal stress and (b) shear stress
versus apparent effective normal stress. When thoroughly dried, montmoril-
lonite is strong (μ ≥ 0.7). The water-saturated, equilibrated field from figure
11.7b is considered to define the true strength of wet montmorillonite. Those
reported values of μ intermediate between the dry and wet strengths are la-
beled "Partially Saturated," and those with apparent friction coefficients lower
than the equilibrium value at a given effective normal stress are labeled "Over-
pressured" (see text). In the overpressured field the reported effective normal
stress may be higher than the true value, because of excess fluid pressures that
are not accounted for. Key: solid green squares, this study; red and yellow ver-
tical bars, see figure 11.8; D, experiments run on reportedly dried montmoril-
lonite samples (drying procedures vary); solid circles, Na-montmorillonite;
open circles, Ca-montmorillonite, with colors: green, *Morrow et al.* [2000];
dark blue, *Morrow et al.* [1992]; light green, *Morrow et al.* [1982]; aqua, *Bird*
[1984], where I, II, and III experiments were run on samples equilibrated at
relative humidities specified by the numbers in parentheses; brownish orange,
Summers and Byerlee [1977a, 1977b], for which samples labeled G were dried
for a longer time than those labeled S and samples labeled w were run wet;
yellow, *Wang et al.* [1980]; black, *Saffer et al.* [2001]; dark gray, *Saffer and
Marone* [2003]; red, *Brown et al.* [2003]; magenta, *Logan and Rauenzahn*
[1987]; light gray, *Shimamoto and Logan* [1981]; lavender, D. A. Lockner and
H. Tanaka (manuscript in preparation, 2006).

minerals, *Byerlee* [1978] found that, with the major exception of the sheet-sili-
cate minerals, μ = 0.80–0.85 at normal stresses ≤200 MPa, and μ tended to
decrease somewhat at higher stresses. These trends, known as Byerlee's law,
are included in figure 11.10a and they should provide the upper limit for dry
montmorillonite strength. For reference, a horizontal line was added at μ =
0.06, the lower limit of reported values. These data (excluding the experiments
using saline pore fluids) are recast in figure 11.10b in a plot of shear stress
versus apparent effective normal stress, with the dry and saturated fields rep-
resented by dashed green lines.

A few data points from studies not included in figure 11.7b plot in the satu-
rated field of figure 11.10a, but most fall well outside it. As discussed below,
the data that plot between the dry and water-saturated regions are interpreted
to represent a "partially saturated" state in which the operative friction mech-
anisms may be a mixture of those characteristic of dry and water-saturated
gouge. Those data plotting between the saturated field and the μ = 0.06 line
may have developed fluid overpressures ("overpressured") that were not al-
leviated over the duration of the experiments.

Partially Saturated   Montmorillonite exposed to room air incorporates atmo-
spheric water onto its crystal surfaces and interlamellar spaces. As the vapor

(a)

(b)
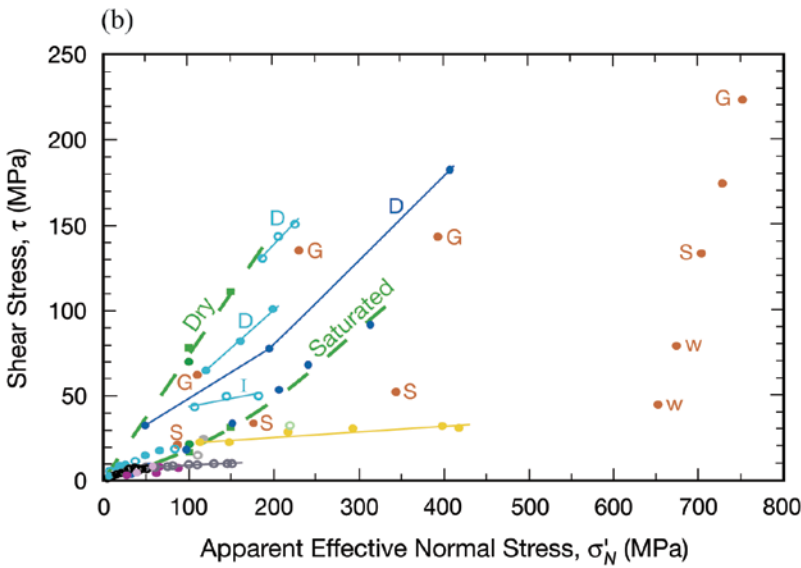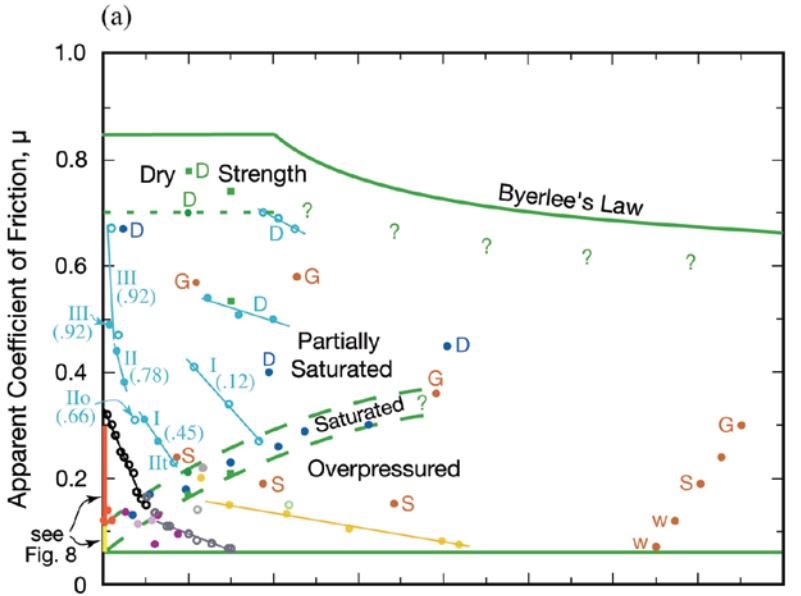
solid symbols: Na-montmorillonite   ○ open symbols: Ca-montmorillonite

■ This study	● Logan and Rauenzahn (1987)
● Brown et al. (2003)	○● Bird (1984)
○ Saffer and Marone (2003)	○ Morrow et al. (1982)
○ Saffer et al. (2001)	○● Shimamoto and Logan (1981)
● Morrow et al. (2000)	● Wang et al. (1980)
● Morrow et al. (1992)	● Summers and Byerlee (1977a, b)

● Lockner and Tanaka, in prep.

pressure of air in contact with a montmorillonite grain rises, the interlayer-water content increases in discontinuous steps, whereas the amount of water adsorbed onto the crystal surfaces increases continuously up to its saturation level [*Newman*, 1987]. With respect to the interlayer water, the transition from a one- to a two-layer structure in Na-montmorillonite occurred at a relative humidity, p/p_o between 0.5 and 0.6, and a uniform three-layer structure at $p/p_o > 0.95$ [*Newman*, 1987]. *Ormerod and Newman* [1983] determined that the water sorption on the external surfaces of montmorillonite is similar to that on reference oxides [*Hagymassy et al.*, 1969]. The equivalent of 1 monolayer is adsorbed onto the external surfaces of those oxides at p/p_o between 0.1 and 0.25, 2 at $p/p_o \approx 0.6$, 3 at $p/p_o \approx 0.85$, and about six monolayers at saturation [*Hagymassy et al.*, 1969].

At a specific vapor pressure, the total amount of water taken on by a smectite clay is a function of the mineral composition and particle size, the size controlling the proportion of surface to interlamellar area [*Newman*, 1987]. Because of its typically very fine grain size [e.g., *Güven*, 1988; *Tournassat et al.*, 2003] and correspondingly large proportion of external surface area, much of the water adsorbed by montmorillonite is external rather than interlayer water [*Newman*, 1987]. The very high specific surface area of montmorillonite compared to other minerals (e.g., 700–800 m^2/g for montmorillonite compared to 100–200 m^2/g for illite and only 5–20 m^2/g for kaolinite [*Fripiat*, 1965]) also means that a room-dry montmorillonite sample will have a significantly larger adsorbed-water content than an illite or kaolinite sample stored at the same room humidity. As a result, montmorillonite and other smectite clays may be much more sensitive than other phyllosilicates to all features of the experimental assembly and procedures that can affect the pore-fluid system.

As a room-dry montmorillonite gouge is compacted, the amount of void space decreases and the water adsorbed onto the surfaces fills a greater proportion of the remaining space. At a sufficiently high normal stress the gouge may become fully saturated [*Wang et al.*, 1980]. Potentially, montmorillonite could also lose some of its interlayer water to unsaturated pore space under high normal loads [*Bird*, 1984, *Colten-Bradley*, 1987]. *Wang et al.* [1980] introduced this hypothesis to explain the compressibility and strength data they obtained on cylinders of packed montmorillonite. They found an abrupt decrease in the rate of compaction of the montmorillonite cylinders at ~200 MPa, corresponding to a volumetric strain of ~12%. On the basis of their estimates of initial porosity (≈20%) and measurements of adsorbed-water content (≈5–7 wt %) of the montmorillonite, they concluded that below 200 MPa much of the decrease in volume was because of the elimination of empty pores and that the change in compressibility was caused by the attainment of water saturation in the sample. In subsequent shearing experiments at confining pressures below 200 MPa, the montmorillonite cylinders showed a small net decrease in volume, consistent with the collapse of empty pores. In contrast, during higher-pressure strength tests the volume remained virtually constant

to ~90% of peak strength [*Wang et al.*, 1980]. The exact frictional mechanisms operative in a partially saturated gouge are not known, but because of the presence of some unfilled void space, they may possibly be a mixture of those characteristic of dry and water-saturated conditions.

On the basis of the hypothesis of *Wang et al.* [1980], a montmorillonite sample equilibrated at high relative humidity should reach water saturation at lower applied normal stresses than one equilibrated at a lower humidity. Conversely, at a given normal stress in an experiment conducted under partially saturated conditions, the montmorillonite gouge equilibrated at a higher relative humidity should have somewhat lower frictional strength. This latter relation has been demonstrated experimentally for the serpentine mineral antigorite by *Reinen et al.* [1994], and the values of μ that they obtained for partially saturated antigorite are all intermediate between the dry and water-saturated antigorite-gouge strengths measured by *Morrow et al.* [2000]. *Horn and Deere* [1962] also found substantial decreases in μ with increasing water content between oven-dried (105°C) and water-saturated serpentine as well as muscovite, phlogopite, biotite, chlorite, and talc. In the same way, the difference in strength between the two granite/granite samples in figure 11.4b can be explained by the lower drying temperature of the weaker sample, although the possibility that trace amounts of water reached the weaker gouge layer during the experiment cannot be ruled out.

The various sets of experimental data that plot in the partially saturated region of figure 11.10a are all consistent with this hypothesis. The majority of the unsaturated data points come from the paper by *Bird* [1984], who tested a sodium-rich (solid circles in figure 11.10) and a calcium-rich (open circles) montmorillonite in a triaxial apparatus without applied fluid pressure. The gouge samples were equilibrated at humidity levels that he had determined from X-ray diffraction analysis should yield montmorillonite containing 0, 1, 2, or 3 water interlayers (labeled D, I, II for Na-montmorillonite and IIt and IIo for Ca-montmorillonite, and III, respectively, in fig. 11.10a). From comparison of figures 2, 3, and 9 in *Bird*'s [1984] paper, the relative humidities used to prepare specific samples were as follows: 0.12 = Ca-montmorillonite I; 0.45 = Ca-montmorillonite IIt and Na-montmorillonite I; 0.66 = Ca-montmorillonite IIo; 0.78 = Na-montmorillonite II; and 0.92 = Ca- and Na-montmorillonite III. His thesis was that shear of montmorillonite was concentrated in the interlayers, and strength decreased with increasing hydration of the interlayer. He did not consider the possibility of shear through surface-adsorbed water films. However, the data are completely consistent with the hypothesis proposed here. In all cases the coefficient of friction of montmorillonite gouge equilibrated at a specific humidity level decreases linearly with increasing σ_n'. The trend for the Group I Ca-montmorillonite samples ($p/p_o = 0.12$) intersects the saturated field at a higher normal stress than the Group I Na-montmorillonites and IIt Ca-montmorillonite equilibrated at $p/p_o = 0.45$. The three Group III samples ($p/p_o = 0.92$), both Ca- and Na-montmorillonite, also have com-

parable strength behavior, and the extrapolated linear trend of the Group III data would intersect the saturated field at the lowest normal stresses of the set. The dry Na-montmorillonite samples are unusual in that they are weaker than both the dry Ca-montmorillonites and the Na-montmorillonites that define the dry strength field in figure 11.10a. Even so, they are considerably stronger than the Group I Ca-montmorillonites ($p/p_o = 0.12$), which were tested over the same range of normal stresses. Na-montmorillonite takes on water more readily than does Ca-montmorillonite [e.g., *Keller et al.*, 1986], and *Bird*'s [1984] dry Na-montmorillonite may have contained traces of adsorbed water.

Saffer et al. [2001] ran direct-shear friction experiments on a room-dry Ca-smectite with 11 wt % water (presumably the nonstructural water content). Their strength data follow a linear trend of decreasing µ with increasing σ_n' similar to the trends of *Bird*'s [1984] data, and they noted a transition in velocity dependence from velocity weakening at velocities <20 µm/s for normal stresses below 30–40 MPa to exclusively velocity-strengthening behavior at higher normal stresses. Their 40–50 MPa results plot within or adjacent to the saturated field, which suggests that the transition in velocity dependence may be a function of the degree of water-saturation of the samples. A shift from velocity-weakening to velocity-strengthening behavior with increasing humidity was reported for antigorite by *Reinen et al.* [1994]. D. A. Lockner and H. Tanaka (manuscript in preparation, 2006) measured exclusively velocity-strengthening behavior for saturated montmorillonite gouge at 40 and 60 MPa σ_n' and velocities in the range 0.0001 to 10 µm/s.

Drying temperatures above 100°C are needed to completely remove the adsorbed water from montmorillonite [e.g., *Mackenzie*, 1957; *Deer et al.*, 1962], and the coefficients of friction of three samples of montmorillonite gouge that *Morrow et al.* [1992] dried at 100°C before testing without applied fluid pressure all plot in the unsaturated rather than the dry field in figure 11.10a. These three data points do not define a linear trend, perhaps reflecting differences in sample treatment after drying.

Summers and Byerlee [1977b] ran two sets of strength experiments on montmorillonite gouge at confining pressures of ~73, 155, 312, and 625 MPa. The samples were vacuum dried at an unspecified temperature, with one group being dried for an unspecified shorter period of time (labeled S) than the other (labeled G). In all cases, the sample with the greater drying time was stronger than the one with the shorter drying time tested at the same confining pressure. The two lowest-pressure G samples and the lowest-pressure S sample plot in the partially saturated field.

Overpressured   The development of fluid overpressures was proposed by *Wang et al.* [1980] to explain the lack of change in the shear strength of cylinders of compacted montmorillonite with increasing confining pressure (fig. 11.10b). Their sample configuration did not allow any loss of fluid; brass disks were placed on the ends of the montmorillonite cylinders, and the whole assembly was then

covered with liquid rubber. (Note that the data plotted in fig. 11.10 from the *Wang et al*. [1980] paper are the peak strengths of the experiments.) As described previously, the results of compaction tests on the montmorillonite cylinders suggested to *Wang et al*. [1980] that the samples reached fluid-saturated conditions at ≤200 MPa confining pressure. They concluded that further increases in confining pressure were matched by increases in pore pressure to maintain a constant effective pressure. On the basis of their interpretation, the reported effective normal stresses of the data in the overpressured field in figure 11.10a are higher than the true values. In consequence, the coefficients of friction calculated using those numbers (figure 11.10a) would be lower than the true values.

The sample assemblies and test conditions of all the experiments plotting in the overpressured field will favor the development of fluid overpressures. *Saffer and Marone* [2003] extended the velocity-stepping experiments of *Saffer et al*. [2001] to higher normal stresses, using the same Ca-montmorillonite starting material and sliding velocities of 1–200 µm/s. In their direct-shear experimental apparatus the room-dry clay was placed between steel forcing blocks. Although water could escape from the edges of the sample, the time constant for fluid-pressure equilibration in this sample geometry would probably exceed many of the test sequence times.

As a comparison, the decay times for reducing a 1-MPa pore-pressure transient in a clay layer were estimated for the triaxial apparatus in figure 11.3 and the direct-shear setup of *Saffer and Marone* [2003]. For both cases a storage capacity of 10^{-3} MPa^{-1} was assumed, so that an imposed volumetric strain of 10^{-3} would result in a 1-MPa pore-pressure change. For the sawcut triaxial geometry this pressure pulse is dissipated by flow of fluid across the gouge layer to the sandstone driving block (<0.1 cm). Using a permeability of 10^{-6} darcy ($\approx 10^{-18}$ m^2), the time needed to reduce the pore pressure transient across a 0.1-cm gouge layer by 80% is on the order of 1 s [*Carslaw and Jaeger*, 1984, p. 101]. *Saffer and Marone* [2003] did not provide the lateral dimensions of their gouge layers, but *Frye and Marone* [2002] reported a sample size of 10 cm × 10 cm for experiments conducted in the same direct-shear apparatus. For diffusion problems of this type, decay timescales approximately as (distance)^2. In the direct shear apparatus, the gouge layer is open to air at the edges, and dissipation of overpressured fluid in the center of the sample would require a radial flow path of ~5 cm. In this case, the time required for a 1-MPa pressure pulse to decay by 80% [*Carslaw and Jaeger*, 1984, p. 200] would be >15 min. Consequently, rapid deformation tests could be complicated by the presence of unknown internal pore pressures. From figure 11.10a, the *Saffer and Marone* [2003] montmorillonite gouge is inferred to have reached saturation at 40–50 MPa σ_n' and to have entered the overpressured field above 60 MPa. The trend of their 60–150 MPa σ_n' data in figure 11.10b parallels that of the *Wang et al*. [1980] experiments at lower shear stresses consistent with the larger adsorbed-water content of their montmorillonite and the fact that *Wang et al*. [1980] reported peak rather than residual strengths.

Summers and Byerlee [1977a, 1977b] used granite forcing blocks for their montmorillonite-gouge strength experiments. The low granite permeability will significantly slow the rate of fluid-pressure equilibration, as illustrated in reverse by the two granite/granite experiments in figure 11.4b. Three of the S (fig. 11.10) samples that *Summers and Byerlee* [1977a, 1977b] tested and one of the G samples plot in the overpressured field. *Summers and Byerlee* [1977b] ran two additional experiments at ≈625 MPa confining pressure on wet (w) montmorillonite samples; that is, the gouge layer was placed on the sawcut surface as a slurry and not dried before use. In addition, *Summers and Byerlee* [1977a] tested an air-dried montmorillonite sample at 625 MPa confining pressure. Of the five 625-MPa experiments (fig. 11.10), the two wet samples are the weakest and the oven-dried sample with the greater drying time (G) the strongest. The overall increase in shear strength with increasing "dryness" of the samples (fig. 11.10b) is consistent with the generation of smaller fluid overpressures in the drier samples.

Logan and Rauenzahn [1987] used Tennessee sandstone forcing blocks for their triaxial friction experiments. Tennessee (Crab Orchard) sandstone has a porosity of 2–3% and a permeability of 4×10^{-19} m^2 at 20-MPa effective confining pressure (D. A. Lockner and C. A. Morrow, manuscript in preparation, 2006), which is close to the permeability of Westerly granite. *Logan and Rauenzahn* [1987] saturated their samples with water for 20 hours prior to conducting velocity-stepping experiments without an imposed fluid pressure. Two data points from experiments at 25- and 50-MPa confining pressure plot within the saturated field (fig. 11.10). Another 50-MPa test was run at such high velocities (maximum of 200 μm/s, which was also the maximum velocity of the *Saffer and Marone* [2003] experiments) that it was completed in ~15 min. This sample was considerably weaker than the other one run at 50 MPa, and *Logan and Rauenzahn* [1987] attributed the low strength to the lack of attainment of pore-pressure equilibrium. Their one experiment at 70 MPa confining pressure also plots in the overpressured field.

Two additional data points in the overpressured area are also from experiments conducted using forcing blocks of Westerly granite [*Morrow et al.*, 1982] and Tennessee sandstone [*Shimamoto and Logan*, 1981].

Effect of Pore-Fluid Composition

Most of the experiments investigating the effect of fluid chemistry on montmorillonite strength have been conducted at low-stress conditions (fig. 11.8). These experiments show an overall increase in μ with increasing salinity, although there is some variability in the data for concentrations between ≈0.05 M and 1 M NaCl that may reflect the very different procedures used to control pore-fluid chemistry in those studies. Saline pore fluids will tend to collapse the double layers of water surrounding the montmorillonite grains, which, in

turn, will increase shear strength. A saturated NaCl solution raises μ fourfold to fivefold at these low stresses to a value as high as 0.3, the equivalent of increasing σ_n' to $\approx$250–300 MPa for a montmorillonite gouge equilibrated with deionized water (fig. 11.7b). *Brown et al*. [2003] ran direct-shear experiments at somewhat higher stresses of 2–30 MPa σ_n' (fig. 11.10a) using seawater as pore fluid, which is roughly equivalent to a 0.5 M NaCl solution. Their results for tests at 0.1 μm/s shear rate plot just above the saturated field in figure 11.10a. The effect of changing salinity is expected to be most pronounced at low effective normal stresses, where very low salinity fluids can result in thick films of structured water (fig. 11.7a).

Suggestions for Future Research

Temperature and Velocity Dependence of Montmorillonite Strength

Enough water-saturated, equilibrated friction experiments have been conducted on montmorillonite to determine the stress dependence of μ between 0.1 and 300 MPa σ_n' at room temperature. Although less work has been done on the velocity dependence of montmorillonite strength, the available evidence from this and previous studies [*Morrow et al*., 1992; *Brown et al*., 2003; D. A. Lockner and H. Tanaka, manuscript in preparation, 2006] also suggest that under water-saturated conditions at room temperature, montmorillonite strength consistently increases with increasing velocity. Those data indicating Δμ ≤ 0 with increasing velocity appear to be associated with dry (fig. 11.4) or unsaturated [*Saffer et al*., 2001] experimental conditions. D. A. Lockner and H. Tanaka (manuscript in preparation, 2006) discuss the room-temperature velocity dependence of montmorillonite strength in more detail.

In contrast, no friction experiments have been conducted at elevated temperatures within the stability range of montmorillonite. As noted previously, montmorillonite and chrysotile have similar room-temperature strengths, particularly at high σ_n' (fig. 11.9), and *Moore et al*. [1997, 2004] have shown that heated chrysotile undergoes a minimum of strength at T ≈ 100°C and $\sigma_n' \leq$ 40 MPa (fig. 11.9). If heated montmorillonite and chrysotile also behave similarly, then montmorillonite could potentially become even weaker at some depth interval in a fault zone. The velocity dependence of μ may also vary with temperature, as was observed with chrysotile [*Moore et al*., 1997, 2004]. Because of the importance of montmorillonite in subduction- and other fault-zone settings, the temperature dependence of montmorillonite frictional strength over a wide range of velocities needs to be thoroughly investigated. If possible, such hydrothermal strength experiments should be conducted using realistic fluid compositions, as *Brown et al*. [2003] have done in their room-temperature experiments.

Effects of Fluid and Mineral Composition

All of the experiments in figure 11.7b were run on Na-montmorillonite. The nature of the interlayer cation might be expected to have little effect on montmorillonite strength, but the strength behavior of Ca- and Na-montmorillonite has been directly compared under water-saturated, equilibrated conditions only in the investigation conducted by *Kenney* [1967] at 0.1 MPa effective normal stress. In identical experiments run using pure water as pore fluid, he found that the coefficient of friction of Ca-montmorillonite was about twice the value for Na-montmorillonite [*Kenney*, 1967]. However, the strength of the Ca-montmorillonite was essentially unaffected by the use of a saturated solution of $CaSO_2$ as pore fluid [*Kenney*, 1967], whereas that of Na-montmorillonite doubled when deioned water was replaced by ≈0.5 M NaCl solution (fig. 11.8). The very low-stress conditions of the experiments may have influenced the effect of fluid chemistry on Na-montmorillonite strength, and experiments at higher effective stresses more appropriate for fault zones need to be conducted. For example, *Alcantar et al.* [2003] found that at normal loads >10 MPa, the thickness of a water film between two muscovite sheets increases with increasing salinity. In their experiments, NaCl solutions had a markedly different effect on water-film thickness than $CaCl_2$ solutions.

Kenney [1967] tested Ca-montmorillonite in a Ca-rich fluid and Na-montmorillonite in Na-rich fluid. Similarly, *Brown et al*. [2003] used Na-rich seawater for their strength experiments on Na-montmorillonite. Fluid chemistry, in particular the cation species in solution [e.g., *Alcantar et al.*, 2003], may have an effect on the strength of the smectite clays and should be investigated. Such studies would have application to montmorillonite-rich rock units cut by and incorporated into fault zones in which the migrating fluids have very different chemistry from those present when the clays formed. Changing fluid chemistry with time during the earthquake cycle may also influence frictional behavior.

Because of differences in their crystal structures and compositions [*Deer et al.*, 1962], the frictional strengths of other smectite clays may differ somewhat from that of montmorillonite. On the basis of their ideal compositions, the predicted values of μ at 100 MPa σ_n' for beidellite and (1) nontronite, (2) hectorite, and (3) saponite are indicated by the open squares in figure 11.6. Of these, the combination of negative tetrahedral-sheet charge and dioctahedral character should make beidellite and nontronite the strongest of the smectite minerals, whereas the trioctahedral character and lack of tetrahedral-sheet charge should make hectorite the weakest. Montmorillonite and saponite are expected to have similar strengths that at 100 MPa σ_n' may be ≈50% lower than for beidellite and nontronite (fig. 11.6). These predictions can be readily tested in laboratory friction experiments.

The Smectite-to-Illite Transition

The smectite-to-illite replacement reaction has been documented in numerous fault-zone settings [e.g., *Tribble*, 1990; *Vrolijk and van der Pluijm*, 1999; *Brown*

et al., 2003], and it has been hypothesized to influence fault-zone rheology in various ways. Laboratory experiments designed to investigate the implications of this reaction for fault strength typically are conducted on mixtures of montmorillonite and disaggregated illite-rich shales [e.g., *Morrow et al.*, 1992; *Brown et al.*, 2003; *Saffer and Marone*, 2003]. Although such mixtures may provide a reasonable estimate of the strength of a mixed-layer illite-smectite clay, at least one comparative study using natural mixed-layer clays should be conducted to verify this assumption. The reason for doing this is that some mechanisms proposed for the illitization of smectite clays involve the formation of intermediate clay structures with different chemical and crystallographic properties and, in consequence, potentially different frictional behavior. *Boles and Franks* [1979] considered the chemical environment for the replacement reaction to be a closed system with enough K available in detrital K-feldspar and mica grains for easy acquisition by the smectite, and K-Na exchange may have preceded Al-Si exchange. They proposed that the newly formed illite occurs as separate packets rather than in a sequence of alternating layers with smectite. Such reaction products should be adequately represented in strength experiments by mixtures of illite and smectite. In contrast, *Bell* [1986] proposed that Al from the octahedral sheet of smectite first replaces Si in the tetrahedral sheet to form an illite-like tetrahedral sheet. He also considered the reaction environment to be an open system in which many partly altered smectites contain high-charge layers but lack the K to convert them completely to illite. Such clays would have a high swelling potential indicating a large percentage of smectite, but their frictional strengths might be more similar to illite than smectite clays, because of the large tetrahedral-sheet charge (fig. 11.6).

The smectite-to-illite reaction has been proposed as the cause of the onset of seismicity at shallow depths in subduction zones [*Vrolijk*, 1990]. However, the smectite-clay content of sediments entering different subduction zones is highly variable [e.g., *Hyndman et al.*, 1997], and smectite abundance can also vary substantially along strike within a subduction zone [*Underwood*, 2002]. Because of this, a more general process than the replacement of smectite clay by illite is required to explain earthquake generation at relatively shallow depths in subduction zones. *Moore and Saffer* [2001] emphasized that the temperature range of the smectite-to-illite transition is characterized by a variety of diagenetic to low-grade metamorphic reactions and processes that will tend to lithify and thereby strengthen the sediments [see also *Brown et al.*, 2003]. As one of the possible reactions involved in this lithification process, understanding the overall smectite-to-illite reaction is important in terms of the changes in mineral assemblage, porosity structure, and fabric development and their combined effect on density, permeability, strength, and sliding stability of the sediments. For example, the formation of illite from smectite and K-feldspar yields SiO_2 as a reaction product [e.g., *Abercrombie et al.*, 1994] that likely will be deposited in the pore spaces of the sediment, affecting strength and perhaps sliding stability. Experiments designed to study the evolution of the rheological properties of marine sediments under hydro-

thermal conditions should provide important information about the onset of seismicity in subduction zones.

Conclusions

Our work on the frictional behavior of thoroughly dry and water-saturated montmorillonite, combined with the hypotheses of *Wang et al.* [1980], provides a possible framework for reconciling the disparate friction data published to date on that important mineral. These interpretations should be tested further under well-controlled experimental conditions to determine their validity. Nevertheless, this work demonstrates that in order to advance our understanding of the frictional properties of montmorillonite and other smectite clays under conditions applicable to fault zones, future research should be conducted only on fluid-saturated samples using experimental assemblies and procedures that will ensure that the fluid pressures remain equilibrated. Study of the interplay of temperature, mineral and fluid chemistry, and effective stress in influencing smectite-clay frictional behavior may be critical to proper understanding of the role of these minerals in fault zones.

References

Abercrombie, H. J., I. E. Hutcheon, J. D. Bloch, and P. de Caritat (1994), Silica activity and the smectite-illite reaction, *Geology, 22*(6), 539–542.

Alcantar, N., J. Israelachvili, and J. Boles (2003), Forces and ionic transport between mica surfaces: Implications for pressure solution, *Geochim. Cosmochim. Acta, 67*, 1289–1304.

Bell, T. E. (1986), Microstructure in mixed-layer illite/smectite and its relationship to the reaction of smectite to illite, *Clays Clay Miner., 34*, 146–154.

Bird, P. (1984), Hydration-phase diagrams and friction of montmorillonite under laboratory and geologic conditions, with implications for shale compaction, slope stability, and fault gouge, *Tectonophysics, 107*, 235–260.

Bish, D. L., and R. F. Giese Jr. (1981), Interlayer bonding in IIb chlorite, *Am. Mineral., 66*, 1216–1220.

Bleam, W. F. (1990), The nature of cation-substitution sites in phyllosilicates, *Clays Clay Miner., 38*, 527–536.

Boles, J. R., and S. G. Franks (1979), Clay diagenesis in Wilcox sandstones of southeast Texas: Implications of smectite diagenesis on sandstone cementation, *J. Sediment. Petrol., 49*, 55–70.

Brown, K. M., A. Kopf, M. B. Underwood, and J. L. Weinberger (2003), Compositional and fluid pressure controls on the state of stress on the Nankai subduction thrust: A weak plate boundary, *Earth Planet. Sci. Lett., 214*, 589–603.

Byerlee, J. (1978), Friction of rocks, *Pure Appl. Geophys., 116*, 615–626.

Capet, X., H. Chamley, C. Beck, and T. Holtzapffel (1990), Clay mineralogy of sites 671 and 672, Barbados Ridge accretionary complex and Atlantic abyssal basin: Paleoenvironmental and diagenetic implications, *Proc. Ocean Drill. Program Sci. Results, 110*, 345–363.

Carslaw, H. S., and J. C. Jaeger (1984), *Conduction of Heat in Solids*, 2nd ed., 510 pp., Clarendon, Oxford, U.K.

Chamley, H., J. P. Cadet, and J. Charvet (1986), Nankai trough and Japan trench late Cenozoic paleoenvironments deduced from clay mineralogical data, *Initial Rep. Deep Sea Drill. Proj., 87*, 633–641.

Colten-Bradley, V. A. (1987), Role of pressure in smectite dehydration — Effects on geopressure and smectite-to-illite transformation, *Am. Assoc. Petrol. Geol. Bull., 71*, 1414–1427.

Deer, W. A., R. A. Howie, and J. Zussman (1962), *Rock-Forming Minerals,* vol. 3, *Sheet Silicates*, 270 pp., John Wiley, Hoboken, N. J.

Fripiat, J. J. (1965), Surface chemistry and soil science, in Experimental Pedology, *Proceedings of the Eleventh Easter School in Agricultural Science*, edited by E. G. Hallsworth and D. V. Crawford, pp. 3–13, Butterworths, London.

Frye, K. M., and C. Marone (2002), Effect of humidity on granular friction at room temperature, *J. Geophys. Res., 107*(B11), 2309, doi:10.1029/2001JB000654.

Giese, R. F., Jr. (1978), The electrostatic interlayer forces of layer structure minerals, *Clays Clay Miner., 26*, 51–57.

Giese, R. F., Jr. (1980), Hydroxyl orientations and interlayer bonding in amesite, *Clays Clay Miner., 28*, 81–86.

Grim, R. E., and N. Güven (1978), Bentonites. Geology, mineralogy, properties and uses, *Dev. Sediment, 24*, 256 pp.

Güven, N. (1988), Smectites, in hydrous phyllosilicates (exclusive of micas), *Rev. Mineral, 19*, 497–559.

Güven, N. (1992), Molecular aspects of clay-water interactions, in *Clay-Water Interface and Its Rheological Implications*, edited by N. Güven, *Clay Min. Soc. Workshop Lect., 4*, 1–79.

Hagymassy, J., Jr., S. Brunauer, and R. S. Mikhail (1969), Pore structure analysis by water vapor adsorption I. t-curves for water vapor, *J. Colloid Interface Sci., 29*, 485–491.

Horn, H. M., and D. U. Deere (1962), Frictional characteristics of minerals, *Geotechnique, 12*, 319–335.

Hyndman, R. D., M. Yamano, and D. A. Oleskevich, (1997), The seismogenic zone of subduction thrust earthquakes, *Island Arc, 6*, 244–260.

Israelachvili, J. N., P. M. McGuiggan, and A. M. Homola (1988), Dynamic properties of molecularly thin liquid films, *Science, 240*, 189–191.

Keller, W. D., R. C. Reynolds, and A. Inoue (1986), Morphology of clay minerals in the smectite-to-illite conversion series by scanning electron microscopy, *Clays Clay Miner, 34*, 187–197.

Kenney, T. C. (1967), The influence of mineral composition on the residual strength of natural soils, in *Proceedings of the Geotechnical Conference on Shear Strength Properties of Natural Soils and Rocks, Oslo, Norway 1967*, pp. 123–129, Norwegian Geotechnical Institute, Oslo.

Liechti, R., and M. D. Zoback (1979), Preliminary analysis of clay gouge from a well in the San Andreas fault zone in central California, *Proceedings of Conference VIII, Analysis of Actual Fault Zones in Bedrock*, *U. S. Geol. Surv. Open File Rep., 79-1239*, 269.

Logan, J. M., and K. A. Rauenzahn (1987), Frictional dependence of gouge mixtures of quartz and montmorillonite on velocity, composition, and fabric, *Tectonophysics, 144*, 87–108.

Lupini, J. F., A. E. Skinner, and P. R. Vaughan (1981), The drained residual strength of cohesive soils, *Geotechnique, 31*, 181–213.

Mackenzie, R. C., ed. (1957), *The Differential Thermal Analysis of Clays*, 456 pp., Mineral Soc., London.

Maio, C. Di, and G. B. Fenelli (1994), Residual strength of kaolin and bentonite: The influence of their constituent pore fluid, *Geotechnique, 44*, 217–226.

Moore, D. E., and D. A. Lockner (2004), Crystallographic controls on the frictional behavior of dry and water-saturated sheet-structure minerals, *J. Geophys. Res., 109*, B03401, doi:10.1029/2003JB002582.

Moore, D. E., D. A. Lockner, M. Shengli, R. Summers, and J. D. Byerlee (1997), Strengths of serpentinite gouges at elevated temperatures, *J. Geophys. Res., 102*, 14,787–14,801.

Moore, D. E., D. A. Lockner, H. Tanaka, and K. Iwata (2004), The coefficient of friction of chrysotile gouge at seismogenic depths, *Int. Geol. Rev., 46*, 385–398.

Moore, J. C., and D. Saffer (2001), Updip limit of the seismogenic zone beneath the accretionary prism of southwest Japan: An effect of diagenetic to low-grade metamorphic processes and increasing effective stress, *Geology, 29*(2), 183–186.

Moore, R. (1991), The chemical and mineralogical controls upon the residual strength of pure and natural clays, *Geotechnique, 41*, 35–47.

Morrow, C. A., Z. Bo-Chong, and J. D. Byerlee (1986), Effective pressure law for permeability of Westerly granite under cyclic loading, *J. Geophys. Res., 91*, 3870–3876.

Morrow, C. A., L. Q. Shi, and J. D. Byerlee (1982), Strain hardening and strength of clay-rich fault gouges, *J. Geophys. Res., 87*, 6771–6780.

Morrow, C., B. Radney, and J. Byerlee (1992), Frictional strength and the effective pressure law of montmorillonite and illite clays, in *Fault Mechanisms and Transport Properties of Rocks*, edited by B. Evans and T.-F. Wong, pp. 69–88, Elsevier, New York.

Morrow, C. A., D. E. Moore, and D. A. Lockner (2000), The effect of mineral bond strength and adsorbed water on fault gouge frictional strength, *Geophys. Res. Lett., 27*, 815–818.

Newman, A. C. D. (1987), The interaction of water with clay mineral surfaces, in *Chemistry of Clays and Clay Minerals, Mineral. Soc. Monogr.*, vol. 6, edited by A. C. D. Newman, pp. 237–274, John Wiley, Hoboken, N. J.

Ohtani, T., K. Fujimoto, H. Ito, H. Tanaka, N. Tomida, and T. Higuchi (2000), Fault rocks and past to recent fluid characteristics from the borehole survey of the Nojima fault ruptured in the 1995 Kobe earthquake, southwest Japan, *J. Geophys. Res., 105*, 16,161–16,171.

Ormerod, E. C., and A. C. D. Newman (1983), Water sorption on Ca-saturated clays: II. Internal and external surfaces of montmorillonite, *Clay Miner., 18*, 289–299.

Paterson, M. S. (1978), *Experimental Rock Deformation—The Brittle Field*, 254 pp., Springer, New York.

Pudsey, C. J. (1984), X-ray mineralogy of Miocene and older sediments from Deep Sea Drilling Project Leg 78A, *Init. Rep. Deep Sea Drill. Proj., 78A*, 325–342.

Reinen, L. A., J. D. Weeks, and T. E. Tullis (1994), The frictional behavior of lizardite and antigorite serpentinites: Experiments, constitutive models, and implications for natural faults, *Pure Appl. Geophys., 143*, 317–358.

Renard, F., and P. Ortoleva (1997), Water films at grain-grain contacts: Debye-Hückel, osmotic model of stress, salinity, and mineralogy dependence, *Geochim. Cosmochim. Acta, 61*, 1963–1970.

Rosenqvist, I. T. (1984), The importance of pore-water chemistry on mechanical and engineering properties of clay soils, *Phil. Trans. R. Soc. London, Ser. A, 311*, 369–373.

Saffer, D. M., and C. Marone (2003), Comparison of smectite- and illite-rich gouge frictional properties: Application to the updip limit of the seismogenic zone along subduction megathrusts, *Earth Planet. Sci. Lett., 215*, 219–235.

Saffer, D. M., K. M. Frye, C. Marone, and K. Mair (2001), Laboratory results indicating complex and potentially unstable frictional behavior of smectite clay, *Geophys. Res. Lett., 28*, 2297–2300.

Shimamoto, T., and J. M. Logan (1981), Effects of simulated clay gouges on the sliding behavior of Tennessee sandstone, *Tectonophysics, 75*, 243–255.

Skempton, A. W. (1964), Long-term stability of clay slopes, *Geotechnique, 14*, 77–101.

Skempton, A. W. (1985), Residual strength of clays in landslides, folded strata and the laboratory, *Geotechnique, 35*, 3–18.

Skipper, N. T., K. Refson, and J. D. C. McConnell (1993), Monte Carlo simulations of Mg- and Na-smectites, in *Geochemistry of Clay-Pore Fluid Interactions*, edited by D. A. C. Manning, P. L. Hall, and C. R. Hughes, pp. 40–61, CRC Press, Boca Raton, Fla.

Summers, R., and J. Byerlee (1977a), A note on the effect of fault gouge composition on the stability of frictional sliding, *Int. J. Rock Mech. Min. Sci., 14*, 155–160.

Summers, R., and J. Byerlee (1977b), Summary of results of frictional sliding studies, at confining pressures up to 6.98 kb, in selected rock materials, *U.S. Geol. Surv. Open File Rep., 77–142*, 129 pp.

Tournassat, C., A. Neaman, F. Villéras, D. Bosbach, and L. Charlet (2003), Nanomorphology of montmorillonite particles: Estimation of the clay edge sorption site density by low-pressure gas adsorption and AFM observations, *Am. Mineral., 88*, 1989–1995.

Tribble, J. S. (1990), Clay diagenesis in the Barbados accretionary complex: Potential impact on hydrology and subduction dynamics, *Proc. Ocean Drill. Program Sci. Results, 110*, 97–110.

Underwood, M. B. (2002), Strike-parallel variations in clay minerals and fault vergence in the Cascadia subduction zone, *Geology, 30*(5), 155–158.

Vrolijk, P. (1990), On the mechanical role of smectite in subduction zones, *Geology, 18*(8), 703–707.

Vrolijk, P., and B. A. van der Pluijm (1999), Clay gouge, *J. Struct. Geol., 21*, 1039–1048.

Wang, C.-Y., N.-H. Mao, and F. T. Wu, (1980), Mechanical properties of clays at high pressure, *J. Geophys. Res., 85*, 1462–1468.

Wu, F. T. (1978), Mineralogy and physical nature of clay gouge, *Pure Appl. Geophys., 116*, 655–689.

Wu, F. T., L. Blatter, and H. Roberson (1975), Clay gouges in the San Andreas fault system and their possible implications, *Pure Appl. Geophys., 113*, 87–95.

Zoback, M. D., and J. D. Byerlee (1975), Permeability and effective stress, *Am. Assoc. Petrol. Geol. Bull., 59*, 154–158.